Protective effects of endothelial progenitor cell microvesicles carrying miR-98-5p on angiotensin II-induced rat kidney cell injury

HUADE MAI[1*], ZHIHUA HUANG[2*], XIAODIAN ZHANG[3], YUANYUAN ZHANG[4], JUMING CHEN[1], MINGHUI CHEN[1], YUNBO ZHANG[1], YANLING SONG[1], BINGSHU WANG[3], YUNYUN LIN[4] and SHENHONG GU[1,3]

[1]Department of General Practice, The First Affiliated Hospital of Hainan Medical University, Haikou, Hainan 570102; [2]Hainan Medical University, Haikou, Hainan 570000; [3]Key Laboratory of Tropical Cardiovascular Diseases Research of Hainan Province, Key Laboratory of Emergency and Trauma of Ministry of Education, Research Unit of Island Emergency Medicine of Chinese Academy of Medical Sciences, Hainan Medical University, Haikou, Hainan 571199; [4]Department of Cardiology, The First Affiliated Hospital of Hainan Medical University, Haikou, Hainan 570102, P.R. China

Received January 13, 2022; Accepted August 26, 2022

DOI: 10.3892/etm.2022.11638

Abstract. With the increasing number of patients with hypertensive nephropathy worldwide, it has posed a major threat to health and studies on its treatment and pathogenesis are imminent. The present study investigated the mechanism through which microRNA (miR)-98-5p in microvesicles (MVs) secreted by endothelial progenitor cells (EPCs) is involved in the repair of angiotensin II (Ang II)-induced injury of rat primary renal kidney cells (PRKs). After isolation of rat renal cortical sections, PRKs were isolated by density gradient centrifugation and identified by immunofluorescence staining. Transmission electron microscopy identifies successful separation of Mvs. An in vitro cell injury model was constructed using Ang II. The Gene Expression Omnibus was used to analyze the differentially expressed genes between diabetic rats and normal rats, and the Kyoto Encyclopedia of Genes and Genomes was used to analyze the signaling pathways involved in these differentially expressed genes. Reverse transcription-quantitative PCR was used to analyze the effect of EPC-MVs on the expression of miRNA induced by Ang II, and the levels of target genes and signaling pathway-related proteins involved were analyzed by western blot. luciferase was used to detect the targeted binding of miR-98-5p to insulin-like growth factor 1 receptor (IGF1R). Enzyme-linked immunosorbent assay was used to analyze the effect of EPC-MVs on Ang II-induced oxidative stress and inflammation levels on PRKs. Cell Counting Kit-8 was used to analyze the effect of EPC-MVs on the cell viability of PRKs induced by Ang II. The results showed that treatment of PRKs with Ang II decreased cell viability, whereas oxidative stress and inflammation were increased. However, EPC-MVs alleviated Ang II-induced damage of the PRKs. During this process, the Ang-II-induced downregulation of miR-98-5p was reversed by EPC-MVs, so miR-98-5p may be a key factor regulating the action of EPC-MVs. Dual-luciferase assay confirmed that miR-98-5p targets IGF1R. It was subsequently demonstrated that EPC-MVs overexpressing miR-98-5p promoted phosphorylation of PI3K/Akt/endothelial nitric oxide synthase (eNOS), and inhibited the oxidative stress and inflammation in PRKs, which were reversed by the overexpression of IGF1R. In conclusion, the results of the present study demonstrated that EPC-MVs with high expression of miR-98-5p can activate the PI3K/Akt/eNOS pathway by regulating IGF1R, as well as protect PRKs from Ang II-induced oxidative stress, inflammation and inhibition of cell viability.

Correspondence to: Dr Shenhong Gu, Department of General Practice, The First Affiliated Hospital of Hainan Medical University, The Outpatient and Emergency Building, 31 Longhua Road, Haikou, Hainan 570102, P.R. China
E-mail: renee388@163.com

*Contributed equally

Abbreviations: MVs, microvesicles; EPCs, endothelial progenitor cells; Ang II, angiotensin II; CKD, chronic kidney disease; ROS, reactive oxygen species; MDA, malondialdehyde; GSH, glutathione; SOD, superoxide dismutase; PRKs, primary renal kidney cells; IGF1R, insulin-like growth factor 1 receptor; eNOS, endothelial nitric oxide synthase; KEGG, Kyoto Encyclopedia of Genes and Genomes; FCM, flow cytometry; miRNA/miR, microRNA; ov, overexpression; NC, negative control

Key words: miR-98-5p, hypertensive nephropathy, Ang II, ROS, MVs, inflammation

Introduction

High blood pressure can cause damage to several organs, including the kidneys, this increases the possibility of chronic kidney disease (CKD) in hypertensive patients (1). Endothelial cell injury and decreased regeneration and repair ability have important consequences in patients with renal function

impairment. Endothelial progenitor cells (EPCs) have been shown to promote endothelial repair (2), regulate angiogenesis (3) and have therapeutic effects in patients with acute renal ischemia-reperfusion injury and patients with kidney transplantation (4). Therefore, we hypothesized that EPCs may have a protective effect on renal cells against hypertensive nephropathy. Microvesicles (MVs) are secreted continuously by a variety of cells in the body, such as epithelial, tumor and stem cells, and exist in a variety of body fluids, including blood and urine, where they mediate biological functions (5). There is evidence that the protective effect of EPCs is closely related to the release of MVs (6,7). However, the role and underlying mechanism of EPC-MVs in hypertensive nephropathy are still unclear.

Angiotensin II (Ang II) induces vascular injury and plays a key role in vascular diseases by inducing apoptosis, increasing reactive oxygen species (ROS) levels and promoting oxidative stress responses by inducing the secretion of malondialdehyde (MDA) and decreasing that of glutathione (GSH) and superoxide dismutase (SOD) (8-10). Ang II also promotes the production of inflammatory cytokines, such as IL-6, IL-1β and TNF-α (11-13). Therefore, Ang II-induced damage to primary renal kidney cells (PRKs) can be used to simulate hypertension *in vitro* (14,15).

MicroRNAs (miRNAs/miRs) are small non-coding RNAs that are involved in the progression and treatment of a variety of diseases (16). Among them, miR-98-5p is a key regulator in the development of diabetic nephropathy and can reverse renal fibrosis induced by high glucose (17). miRNAs can suppress the transcription and translation of mRNA by binding to the end of the 3'-untranslated region (3'-UTR) of the Mrna (18). New evidence shows that insulin-like growth factor 1 receptor (IGF1R) is involved in the progression of diabetes (19,20). miRNAs can also affect cell viability, differentiation, migration, oxidative stress and inflammation by regulating a series of downstream signaling pathways (21-23). The activation of endothelial nitric oxide synthase (eNOS) in colon cells promotes the viability of endothelial cells and regulates inflammation (24). The protective effect of PI3K/Akt/eNOS on endothelial cells has been established in numerous studies (25,26). Previous evidence has indicated that miR-98-5p affects apoptosis, inflammation and oxidative stress by regulating the PI3K/Akt signaling pathway (27-29). Moreover, studies have shown that IGF1R can affect the development of diabetes through the PI3K/Akt/eNOS axis (30-32).

In the present study, the potential application of miR-98-5p-MVs in the treatment of hypertensive nephropathy was explored by investigating the protective effect and mechanism of miR-98-5p expressed in EPC-MVs on Ang II-induced PRK injury.

Materials and methods

Animals. A total of 12, 8-week-old male Wistar-Kyoto specific pathogen-free rats weighing 80-120 g were obtained from Beijing Vital River Laboratory Animal Technology Co. Ltd. Rats were placed in a room with a 12-h light/dark cycle and a constant temperature and humidity (temperature, 23±2˚C; humidity, 45±15%) with *ad libitum* access to standard rat food and water in a polystyrene cage. Animal experiments were approved by the Animal Care and Use Committee of Hainan Medical University (Haikou, China; approval no. HYLL-2021-053) and were conducted according to the National Institutes of Health guidelines.

Isolation and culture of PRKs. Rats were euthanized by intraperitoneal injection of pentobarbital sodium (200 mg/kg body weight). The kidneys were removed aseptically and the cortical portion of the kidney was excised. The renal cortex was cut into tissue fragments of <1 mm^3, washed with phosphate-buffered saline (PBS) three times and centrifuged at 1,000 x g at 25˚C for 5 min. The supernatant was then discarded. Tissue fragments were added to collagenase type I solution (Gibco; Thermo Fisher Scientific, Inc.) at a final concentration of 1 g/l, and the tissue fragments were digested at 37˚C for 30 min under oscillation. After filtration through a 200-mesh stainless steel filter, the cells were separated by Ficoll®-Paque PREMIUM (Cat. No. 17-5442-02; GE Healthcare, Uppsala, Sweden) density gradient centrifugation (33). The supernatant was discarded after centrifugation at 1,000 x g at 25˚C for 2 min. The precipitate was mixed with Dulbecco's Modified Eagle Medium/Nutrient Mixture F-12 (DMEM/F12) (Gibco; Thermo Fisher Scientific, Inc.), inoculated in a 6-well plate and cultured at 37˚C with 5% CO_2. After 24 h, the supernatant was replaced with fresh medium, and the unattached renal cells and tissues were discarded. After 48 h, the cells were washed twice with PBS and denoted as PRKs (34,35). PRKs were cultured in DMEM/F12 with 10% Fetal bovine serum (FBS; Gibco) for three generations and treated with Ang II (1 μmol) at 37˚C for 24 h to establish the PRK renal damage model. The concentration used for Ang II was selected based on the study by Nair *et al* (36).

Identification of PRKs. PRKs ($5x10^4$) were inoculated into a 6-well plate (on round glass coverslips; Corning, Inc.) for 24 h. After twice rinses with PBS, Fix with 4% formaldehyde at 25˚C for 10 min. Then, Triton-X-100 (0.1%) was added at 4˚C for 2 h. PRKs were incubated with 1% BSA (Beijing Solarbio Science & Technology Co., Ltd.) for 30 min at 4˚C and then overnight with anti-α-smooth muscle actin (α-SMA) (1:200; ab7817; Abcam) and anti-vimentin (1:250; ab92547; Abcam) antibodies at 4˚C in the dark. After rinsing with PBS three times, the cells were incubated with Alexa Fluor® 488-(1:100; cat. no. ab150077; Abcam) or 647-labeled (1:200; cat. no. ab150075; Abcam) secondary antibodies at 37˚C for 1 h. Then, the cells were mounted with Gold Antifade Mountant with DAPI (ProLong™; Thermo Fisher Scientific, Inc.). Finally, images were captured using a fluorescence microscope (magnification, x400; Leica Microsystems GmbH).

Culture and identification of EPCs. The femur and tibia of the rats were separated, and each bone marrow tube was rinsed with sterile PBS. The resulting mixture was centrifuged (1,000 x g; 25˚C; 5 min), and the EPCs were isolated by Ficoll density gradient centrifugation (1,000 x g; 25˚C; 20 min) and cultured (DMEM with 10% FBS) at 37˚C with 5% CO_2. After 4 days, the medium was exchanged with fresh culture medium, and the adherent cells were cultured for another 3 days (37). According to the manufacturer's instructions, Dil complex

acetylated low-density lipoprotein (Dil-Ac-LDL) staining (Cat. No. IL2140; Beijing Solarbio Science & Technology Co., Ltd.) was used to identify EPCs. The criterion for the suitability of isolated EPCs for subsequent experiments was that the red fluorescence of Dil-Ac-LDL and blue fluorescence (DAPI nuclear staining) of most cells overlapped under a fluorescence microscope (magnification x400). In the co-culture system, PRKs ($1x10^4$) were added to the lower chamber of transwell plates (Corning, Inc.) and incubated at 37˚C for 24 h, after which Ang II (1 μM) and EPCs ($3x10^4$) were added to the upper chamber. The medium in both the upper and lower chambers was DMEM/F12 contained 10% FBS. After incubation for 24 h at 37˚C, cells were used for subsequent experiments. As for the co-culture of PRKs and EPC supernatant, after the supernatant of EPCs ($3x10^4$) was collected, cell debris was removed using a filter (Millipore) and then added to PRKs for culture.

Preparation of EPC-MVs. EPCs were cultured for 7 days as aforementioned, washed twice with PBS, and then serum starved for 12 h. Subsequently, DMEM/F12 containing cultured EPCs was centrifuged at 4˚C for 15 min (1,000 x g), and the supernatant was further centrifuged at 4˚C for 60 min (100,000 x g) for the collection of secreted EPC-MVs. MVs were fixed with glutaraldehyde (2.5%; Beijing Solarbio Science & Technology Co., Ltd.) in the dark at 4˚C for 1 hours, 10 μl was added dropwise to the copper stain at 25˚C for 1 min, and the suspension was removed by filter paper. Subsequently, 10 μl of phosphotungstic acid (1%; Beijing Solarbio Science & Technology Co., Ltd.) was added dropwise to the copper stain at 25˚C for 1 min, and the suspension was removed by filter paper. After drying at 25˚C for 30 min, transmission electron microscopy (TEM) was performed at 80 kV for imaging. In the co-culture system, 50 μg/ml EPC-MVs (38) were added to the top chamber of a Transwell assay plate, and PRKs were added to the bottom chamber as aforementioned and incubated for 24 h.

Gene Expression Omnibus (GEO) analysis. Raw data of GSE110231 dataset (https://www.ncbi.nlm.nih.gov/geo/query/acc.cgi?acc=GSE110231) were downloaded from the GEO website (https://www.ncbi.nlm.nih.gov/geo/) and analyzed. The GSE110231 dataset included three healthy Sprague-Dawley rats (subsample, GSM2983040-2983042) and three diabetic rats (subsample, GSM2983037-2983039). Use Gene Expression Profiling Interactive Analysis 2 (http://gepia2.cancer-pku.cn/#index) to analyze the differential expression of miRNA, and the criteria for differential expression are as follows: $P<0.05$, $\log_2|\text{fold change}|\geq 2$. Kyoto Encyclopedia of Genes and Genomes (KEGG; https://www.genome.jp/kegg/) was used to analyze the influence of related signal transduction on diabetes development in rats.

Cell transfection. Mimic (100 nM), inhibitor (100 nM), negative control mimic (NC; 100 nM), NC inhibitor (100 nM), overexpression (ov) IGF1R pCDNA3.1 plasmid (50 nM) and ov-NC plasmid (50 nM) (all from Sangon Biotech Co., Ltd.) were transfected into PRKs or EPCs with Lipofectamine® 2000 (Invitrogen; Thermo Fisher Scientific, Inc.), according to the manufacturer's instructions, and incubated in the dark for 4 h (37˚C, 5% CO_2). After 24 h (for RT-qPCR analysis) or 48 h (for western blot analysis) of the transfection medium replaced with fresh medium, cells and supernatants were collected for further processing. miR-98-5p mimic and inhibitor sequences are presented in Table I.

Table I. Sequences of miRNAs and reverse transcription-quantitative PCR primers.

A, miRNA sequences

miRNA	Sequence (5'-3')
miR-98-5p mimic	UGAGGUAGUAAGUUGUAUUGUU
miR-98-5p mimic NC	UAUAGAUUGUUGGAGUUGUUAG
miR-98-5p inhibitor	AACAATACAACTTACTACCTCA
miR-98-5p inhibitor NC	CAGUACUUUUGUGUAGUACAA

B, Primer sequences

Primer	Sequence (5'-3')
miR-98-5p-F	ACACTCCAGCTGGGTGAGGTAGTAAGTTGT
miR-98-5p-R	CTCAACTGGTGTCGTGGA
U6-F	CTCGCTTCGGCAGCACA
U6-R	AACGCTTCACGAATTTGCGT
IGF1R-F	CTCTAAGGCCAGAGGTGGAGAATAA
IGF1R-R	TGTGGACGAACTTGTTGGCA
GAPDH-F	TGGGGCCAAAAGGGTCATCA
GAPDH-R	GCAGGATGCATTGCTGACAA

F, forward; R, reverse; miRNA/miR, microRNA; IGF1R, insulin-like growth factor 1 receptor.

Reverse transcription-quantitative (RT-q)PCR. According to the manufacturer's instructions, PRKs were extracted using TRIzol® reagent (Invitrogen; Thermo Fisher Scientific, Inc.). After 10 min of centrifugation at 4˚C (13,000 x g), the precipitate was adsorbed and dissolved with 15 μl diethylpyrocarbonate-treated water and reverse-transcribed into cDNA using a PrimeScript™ RT-PCR Kit (Takara Bio Inc.) according to the manufacturer's protocol. SYBR® Premix Ex Taq™ II kit (Takara Bio Inc.) was used for RT-qPCR analysis with the Applied Biosystems® 7500 Real-Time PCR system (Thermo Fisher Scientific, Inc.). qPCR was carried out under the following conditions: 95˚C for 30 sec, followed by 40 cycles of 95˚C for 3 sec and 60˚C for 30 sec. The primer sequences used for RT-qPCR are presented in Table I. MiR-98-5p and *IGF1R* RNA levels were normalized to those of U6 or glyceraldehyde 3-phosphate dehydrogenase (GAPDH) and calculated using the $2^{-\Delta\Delta Cq}$ method (39).

Western blotting. PRKs were lysed using RIPA lysis buffer (Elabscience Biotechnology, Inc.). Lysate protein

Table II. Details of the antibodies used in western blot analysis.

Antibody	Dilution	Cat. no.	Manufacturer	Application
IGF1R	1:1,000	ab182408	Abcam	Primary antibody
PI3K	1:1,000	ab191606	Abcam	Primary antibody
AKT	1:500	ab8805	Abcam	Primary antibody
p-PI3K	1:500	ab182651	Abcam	Primary antibody
p-AKT	1:500	ab38449	Abcam	Primary antibody
eNOS	1:1,000	PA1-037	Invitrogen; Thermo Fisher Scientific, Inc.	Primary antibody
p-eNOS	1:500	MA5-14957	Invitrogen; Thermo Fisher Scientific, Inc.	Primary antibody
Goat anti-rabbit	1:20,000	ab205718	Abcam	Secondary antibody
GAPDH	1:5,000	ab181602	Abcam	Loading control

p, phosphorylated; eNOS, endothelial nitric oxide synthase; IGF1R, insulin-like growth factor 1 receptor.

concentrations were determined using a BCA protein assay kit (Beijing Solarbio Science & Technology Co., Ltd.) and resolved denatured proteins (20 μg) using 10% SDS-PAGE (Elabscience Biotechnology, Inc.). Protein bands were transferred onto a PVDF membrane at 60 V for 2 h at 4˚C. Then, Ponceau S dye was used to stain the membrane at 25˚C for 5 min. The membrane was blocked with 5% BSA at 25˚C for 2 h, incubated with primary antibodies (anti-IGF1R, anti-PI3K, anti-AKT, anti-p-PI3K, anti-p-AKT, anti-eNOS, anti-p-eNOS) overnight at 4˚C, rinsed with TBS-0.05%Tween 20 buffer (Beijing Solarbio Science & Technology Co., Ltd.) twice, for 10 min each time, and incubated with the secondary antibody (Goat anti-rabbit; Horseradish peroxidase) for 1.5 h at 23±2˚C. Details of the antibodies are shown in Table II. Subsequently, ECL reagent (Thermo Fisher Scientific, Inc.) was used for the chemiluminescence reaction. Finally, the membrane was developed and fixed using a Developer and Fixer Kit (Beyotime Institute of Biotechnology), and the densitometry was quantified using ImageJ software (version 1.8.0; National Institutes of Health, Bethesda, MD, USA).

Cell viability assays. PRKs were digested with trypsin, inoculated in 96-well plates at a density of $0.5x10^4$ cells/well, and cultured for 24 h. The optical density at 490 nm was measured using the Cell Counting Kit-8 reagent (CCK-8; 10 μl/well; Beijing Solarbio Science & Technology Co., Ltd.) at 37˚C for 1 h, added at 0 and 24 h according to the manufacturer's instructions, to evaluate the cell viability.

EPC-MVs and PRK fusion. EPC-MVs were labeled with a lipid membrane-embedded fluorescent dye (PKH26; Sigma-Aldrich; Merck KGaA) prior to co-incubation with PRKs. Briefly, 50 g/ml EPC-MVs were mixed with 2 ml PKH26 ($2x10^{-6}$ M) and incubated at 23±2˚C for 5 min. The labeled mixture was added to 2 ml of 1% BSA and centrifuged at 4˚C for 60 min (120,000 x g), and the precipitate was rinsed with PBS. The precipitate was then suspended in 2 ml DMEM/F12 in 6-well plates and added to PRKs ($2x10^5$/ml) before incubation at 37˚C for 24 h. Finally, 1 μg/ml DAPI was added for nuclear staining at 25˚C for 5 min. Cell images were acquired using a fluorescence microscope (Leica Biosystems).

ROS measurements using flow cytometry (FCM). PRKs ($2x10^5$/ml) were incubated in 6-well plates with 2',7'-dichlorodihydrofluorescein diacetate (1.0 μM; Beijing Solarbio Science & Technology Co., Ltd.) at 37˚C for 15 min. Subsequently, PRKs were washed twice with PBS and analyzed by FCM (FACSCanto II; BD FACSChorus™ software, version: 1.0; BD Biosciences) to detect ROS using a 488-nm laser for excitation and a 535-nm laser for detection.

Enzyme-linked immunosorbent assay (ELISA). PRKs cell supernatant of each subgroup was collected to determine the levels of MDA, GSH, SOD, IL-6, IL-1β and TNF-α. The following kits were used according to the manufacturer's instructions: MDA Content Assay Kit (cat. no. BC0020; Beijing Solarbio Science & Technology Co., Ltd.), Reduced GSH Content Assay Kit (cat. no. BC1175; Beijing Solarbio Science & Technology Co., Ltd.), SOD Activity Assay Kit (cat. no. BC0170; Beijing Solarbio Science & Technology Co., Ltd.), Rat IL-1 beta/IL-1F2 Quantikine ELISA Kit (cat. no. RLB00; R&D Systems), Rat IL-6 Quantikine ELISA kit (cat. no. R6000B; R&D Systems) and Rat TNF-α Quantikine ELISA Kit (cat. no. RTA00; R&D Systems).

Dual-luciferase reporter assay. TargetScan software v7.2 (https://www.targetscan.org/vert_72/) was used to predict the binding sites of miRNA and mRNA. PRKs were transfected with 500 ng each of miR-98-5p mimic or inhibitor and their NCs, 1 μg each of the psi-CHECK2 vector (Promega, Madison, WI, USA) containing wild-type or mutant IGF1R 3'-UTR and 50 ng of the pRL-SV40 reporter vector plasmid (Promega) Using Lipofectamine® 2000. Transfected cells were incubated at 37˚C for 48 h, and luciferase activity was measured using the Dual-Luciferase® Reporter Assay System (Promega Corporation) according to the manufacturer's instructions, and the ratio of firefly to *Renilla* activity was used to normalize firefly luciferase values.

Statistical analysis. All experiments were repeated three times. Data are expressed as the mean ± standard deviation. Differences between multiple groups were assessed using one-way analysis of variance and Bonferroni post hoc test. Student's t-test was used for independent two-group analyses

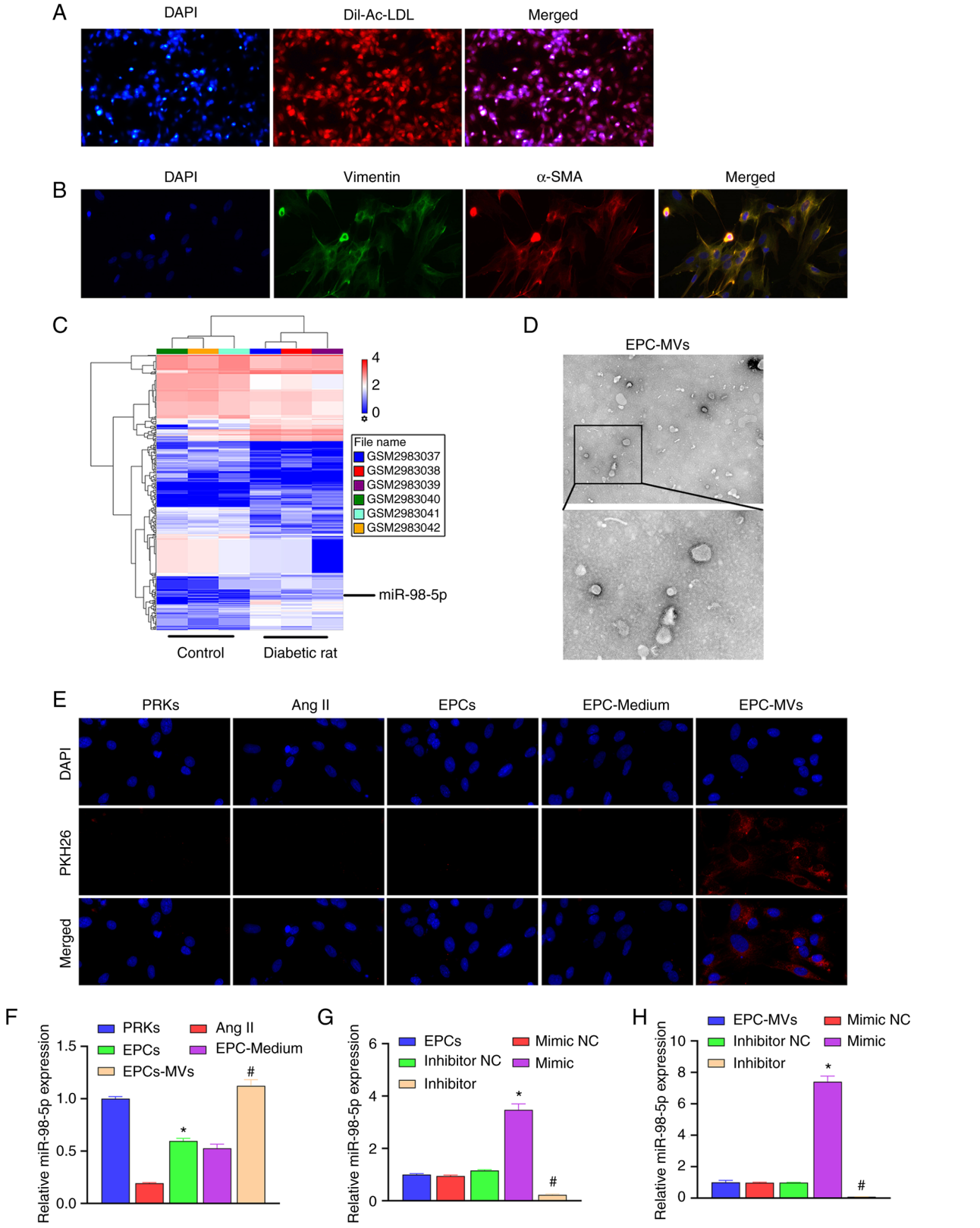

Figure 1. Recovery of Ang II-induced injury of PRKs and co-culture with EPC-MVs. (A) Confirmation of the isolation of EPCs using Dil-Ac-LDL staining (magnification, x100). (B) Confirmation of the isolation of PRKs through immunofluorescence assay (magnification, x400). (C) The GSE110231 dataset was analyzed using Gene Expression Omnibus to screen miRNAs. This heat map shows differentially expressed miRNAs in diabetic rats compared with healthy rats. Blue bands represent low expression, and red bands represent high expression. (D) Analysis of isolated MVs using transmission electron microscopy (upper image magnification, x15,000; lower image magnification, x40,000). (E) PKH26-labeled EPC-MVs successfully fused with PRKs (magnification, x100). (F) RT-qPCR analysis of the impact of Ang II, EPCs, EPC-Medium and EPC-MVs on the expression of miR-98-5p in PRKs (n=3). *P<0.05 vs. Ang II; #P<0.05 vs. EPC-Medium. (G) RT-qPCR analysis of the impact of miR-98-5p mimic/inhibitor transfection on the expression of miR-98-5p in EPCs (n=3). *P<0.05 vs. mimic NC; #P<0.05 vs. inhibitor NC. (H) RT-qPCR analysis of the impact of miR-98-5p mimic/inhibitor transfection on the expression of miR-98-5p in EPC-MVs (n=3). *P<0.05 vs. mimic NC; #P<0.05 vs. inhibitor NC. Dil-Ac-LDL, Dil complex acetylated low-density lipoprotein; Ang II, Angiotensin II; EPCs, endothelial progenitor cells; PRKs, primary renal kidney cells; MVs, microvesicles; RT-qPCR, reverse transcription-quantitative PCR; NC, negative control; α-SMA, α-smooth muscle actin; miR, microRNA.

Table III. List of miRNAs that meet the criteria of $\log_2|FC|\geq 2$ and $P<0.05$.

Transcript identification (array design)	Diabetic rat average ($\log_2$)	Control average ($\log_2$)	Fold change	P-value
rno-miR-1-3p	2.39	4.76	-5.16	0.001
rno-miR-9a-5p	3.37	4.65	-2.43	0.034
rno-miR-98-5p	5.18	6.30	-2.18	0.017
rno-miR-205	4.95	6.78	-3.55	<0.001
rno-miR-206-3p	5.99	7.18	-2.29	0.010
rno-miR-216a-3p	1.23	2.45	-2.34	0.016
rno-miR-219a-2-3p	0.26	1.83	-2.97	0.007
rno-miR-451-5p	3.63	2.34	2.45	0.001
rno-miR-466b-5p	1.83	3.12	-2.44	0.023
rno-miR-490-3p	2.84	1.34	2.84	0.014
rno-miR-743b-3p	3.37	2.33	2.06	0.003
rno-miR-881-3p	4.04	2.65	2.62	0.001
rno-miR-1949	6.47	7.53	-2.08	<0.001

miR, microRNA.

(unpaired). $P<0.05$ was considered to indicate a statistically significant difference using Graphpad prism (Version: 8.0; GraphPad Software Inc.).

Results

Identification of EPCs and PRKs. The isolated EPCs were identified using Dil-Ac-LDL staining. We observed under the fluorescence microscope that most of the cells expressed the superposition of highly positive red fluorescence (Dil-Ac-LDL) and blue fluorescence (nuclear staining with DAPI), which means that the isolated cells are suitable for use in subsequent studies (Fig. 1A). Isolated PRKs were analyzed using immunofluorescence staining (vimentin/α-SMA). The results revealed high expression of vimentin and α-SMA in PRKs, which suggested the successful isolation of PRKs (Fig. 1B).

Analysis and screening of target miRNAs using GEO. To explore the protective mechanism of EPC-MVs against PRK injury, GSE110231 dataset was analyzed using GEO. The results revealed that 430 miRNAs were differentially expressed between the control and the diabetic rat group (Fig. 1C). Among them, 13 miRNAs met the differential expression criteria set in the present study, as shown in Table III. A previous study demonstrated that miR-98-5p expression is reduced in diabetic nephropathy in mice (17). However, the mechanism of miR-98-5p in rat PRKs has not been confirmed. Therefore, miR-98-5p was selected as the target miRNA in the present study.

Transfection of miR-98-5p mimic/inhibitor affects the expression of miR-98-5p in EPC-MVs. The MVs isolated from the culture supernatant of EPCs were observed using TEM (Fig. 1D). Ang II was added to PRK cells to simulate an *in vitro* renal cell injury model, and the protective mechanism of EPCs on Ang II-induced damage of renal cells was further analyzed. EPC-MVs were labeled with PKH26 and incubated with PRKs in the presence of Ang II. PKH26 fluorescence was detected in the cytoplasm of PRKs (Fig. 1E), which indicated the fusion of EPC-MVs with PRKs. RT-qPCR results revealed that Ang II induction reduced the expression of miR-98-5p compared with the control group, which was consistent with the GEO data analysis. The co-culture of PRKs with EPCs or EPC supernatant increased the expression of miR-98-5p, while after treatment with EPC-MVs the expression of miR-98-5p returned to the normal level (Fig. 1F). Subsequently, miR-98-5p mimic and inhibitor were transfected into EPCs. RT-qPCR results revealed that the expression of miR-98-5p was upregulated in the miR-98-5p mimic group, and downregulated in the miR-98-5p inhibitor group compared with their respective controls, which suggested that the transfection with miR-98-5p mimic and inhibitor was successful (Fig. 1G). Additionally, the supernatant of each group was collected and the MVs were extracted. RT-qPCR results revealed that the expression of miR-98-5p in the exosomes of each group was consistent with that in EPCs (Fig. 1H).

miR-98-5p mimic/inhibitor affects PRK viability, oxidative stress and inflammation through EPC-MVs. The collected exosomes from each group were added to the PRKs induced by Ang II. The results revealed that all groups incubated with MVs showed red fluorescence, indicating that the MVs and PRKs were successfully fused (Fig. 2A). CCK-8 analysis revealed that EPC-MVs increased viability of PRKs compared with the Ang II group, and miR-98-5p mimic-MVs enhanced the effect of EPC-MVs, whereas miR-98-5p inhibitor-MVs inhibited the increased cell viability effect of EPC-MVs on PRKs (Fig. 2B). EPC-MVs inhibited Ang II-induced oxidative stress compared with Ang II group [ROS (Fig. 2C, D) and MDA (Fig. 2E) levels decreased, whereas GSH (Fig. 2F) and SOD (Fig. 2G) levels increased] and inflammatory response [IL-1β (Fig. 2H), IL-6 (Fig. 2I) and TNF-α (Fig. 2J)]. Furthermore, co-treatment with miR-98-5p

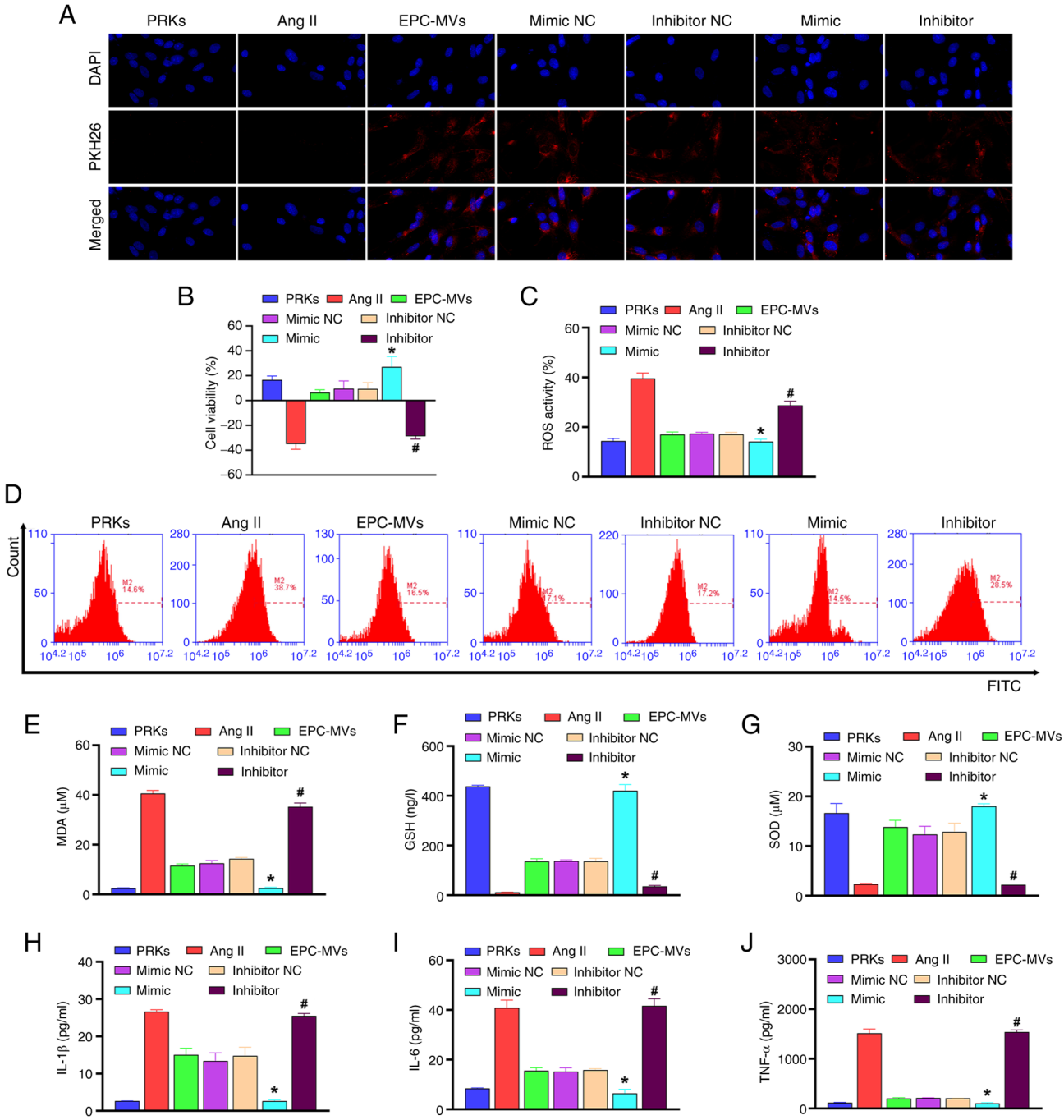

Figure 2. miR-98-5p-MVs inhibit Ang II-induced oxidative stress and the secretion of inflammatory cytokines in PRKs. (A) PKH26-labeled miR-98-5p-MVs successfully fused with PRKs (magnification, x100). (B) Cell Counting Kit-8 analysis determined the effects of miR-98-5p-MVs on the cell viability of PRKs treated with Ang II (n=3). (C and D) Flow cytometry analysis determined the effect of miR-98-5p-MVs on the levels of Ang II-induced ROS production in PRKs (n=3). ELISA analysis determined the effect of miR-98-5p-MVs on the levels of (E) MDA, (F) GSH and (G) SOD in PRKs treated with Ang II (n=3). ELISA analysis determined the effect of miR-98-5p-MVs on the levels of secreted (H) IL-1β, (I) IL-6 and (J) TNF-α in PRKs treated with Ang II (n=3). *P<0.05 vs. mimic NC; #P<0.05 vs. inhibitor NC. Ang II, angiotensin II; ROS, reactive oxygen species; EPCs, endothelial progenitor cells; PRKs, primary renal kidney cells; MVs, microvesicles; MDA, malondialdehyde; GSH, glutathione; SOD, superoxide dismutase; NC, negative control; miR, microRNA.

mimic-MVs enhanced the inhibitory effect of EPC-MVs on oxidative stress and inflammation, whereas co-treatment with miR-98-5p inhibitor-MVs had an opposite effect to that of miR-98-5p mimic-MVs. These results indicated the successful establishment of the Ang II-induced PRK injury model and the injury-repair effect of miR-98-5p mimic-MVs. Therefore, the mechanism of miR-98-5p on Ang II-induced PRK injury was further examined.

Mechanism of miR-98-5p MVs against PRK injury. The results of KEGG analysis indicated that the PI3K-Akt signaling pathway is an important factor affecting the progress of diabetes (Fig. 3A). In the GSE110231 dataset, 16 target genes were identified as key factors affecting the PI3K-Akt signaling pathway. A total of 16 mRNAs were compared with the downstream target genes of miR-98-5p (predicted by the TargetScan database) and it was found that IGF1R was shared between the

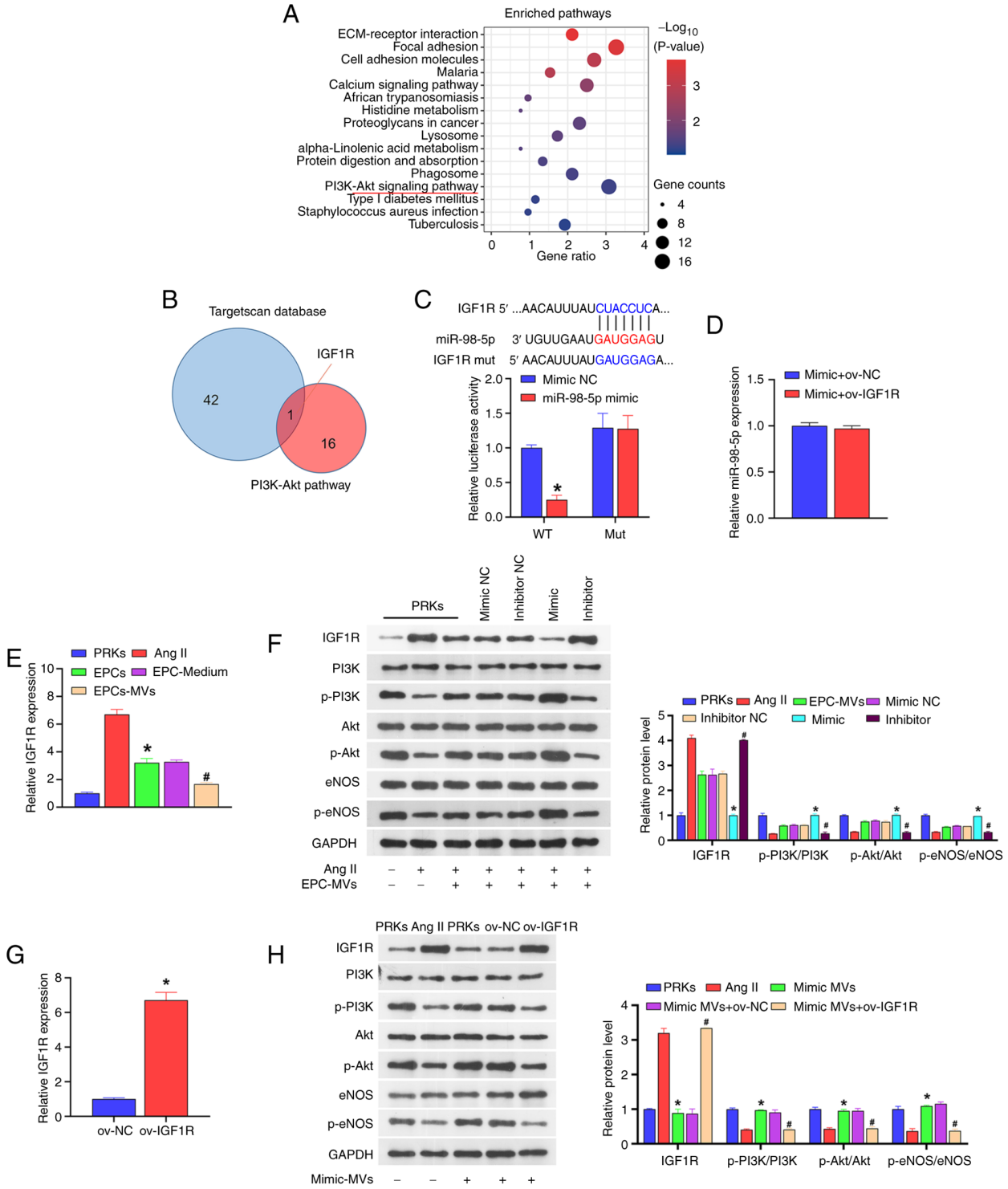

Figure 3. miR-98-5p targets IGF1R to regulate the PI3K/Akt/eNOS signaling pathway. (A) KEGG analysis of the signaling pathways associated with the progression of diabetes. (B) Key factors affecting the PI3K-Akt signaling pathway (result of the KEGG analysis) and TargetScan database were jointly used to screen target genes. (C) Dual-luciferase analysis of the binding of miR-98-5p and the putative target gene IGF1R (n=3) *P<0.05 vs. mimic NC. (D) RT-qPCR analysis of the impact of ov-IGF1R on the expression of miR-98-5p in PRKs (n=3). (E) RT-qPCR analysis the impact of Ang II, EPCs, EPC-Medium and EPC-MVs on the expression of IGF1R in PRKs (n=3). *P<0.05 vs. Ang II; $^{\#}$P<0.05 vs. EPC-Medium. (F) Western blot analysis of the impact of miR-98-5p-MVs on the protein levels of IGF1R, PI3K, p-PI3K, Akt, p-Akt, eNOS and p-eNOS (n=3). *P<0.05 vs. mimic NC; $^{\#}$P<0.05 vs. inhibitor NC. (G) RT-qPCR analysis of IGF1R expression in PRKs after transfection with ov-NC or ov-IGF1R (n=3) *P<0.05 vs. ov-NC. (H) Western blot analysis of the combined effects of miR-98-5p-MVs and IGF1R on the protein levels of IGF1R, PI3K, p-PI3K, Akt, p-Akt, eNOS and p-eNOS (n=3). *P<0.05 vs. Ang II; $^{\#}$P<0.05 vs. mimic-MVs + ov-NC. IGF1R, insulin-like growth factor 1 receptor; eNOS, endothelial nitric oxide synthase; RT-qPCR, reverse transcription-quantitative PCR; Ang II, Angiotensin II; KEGG, Kyoto Encyclopedia of Genes and Genomes; EPCs, endothelial progenitor cells; PRKs, primary renal kidney cells; MVs, microvesicles; p, phosphorylated; NC, negative control; ov, overexpression; WT, wild-type; mut, mutant; miR, microRNA.

two datasets (Fig. 3B). The subsequent dual-luciferase assay result revealed that when wild-type IGF1R was co-transfected with miR-98-5p mimic, the luciferase activity was significantly lower than that of the group co-transfected with mimic

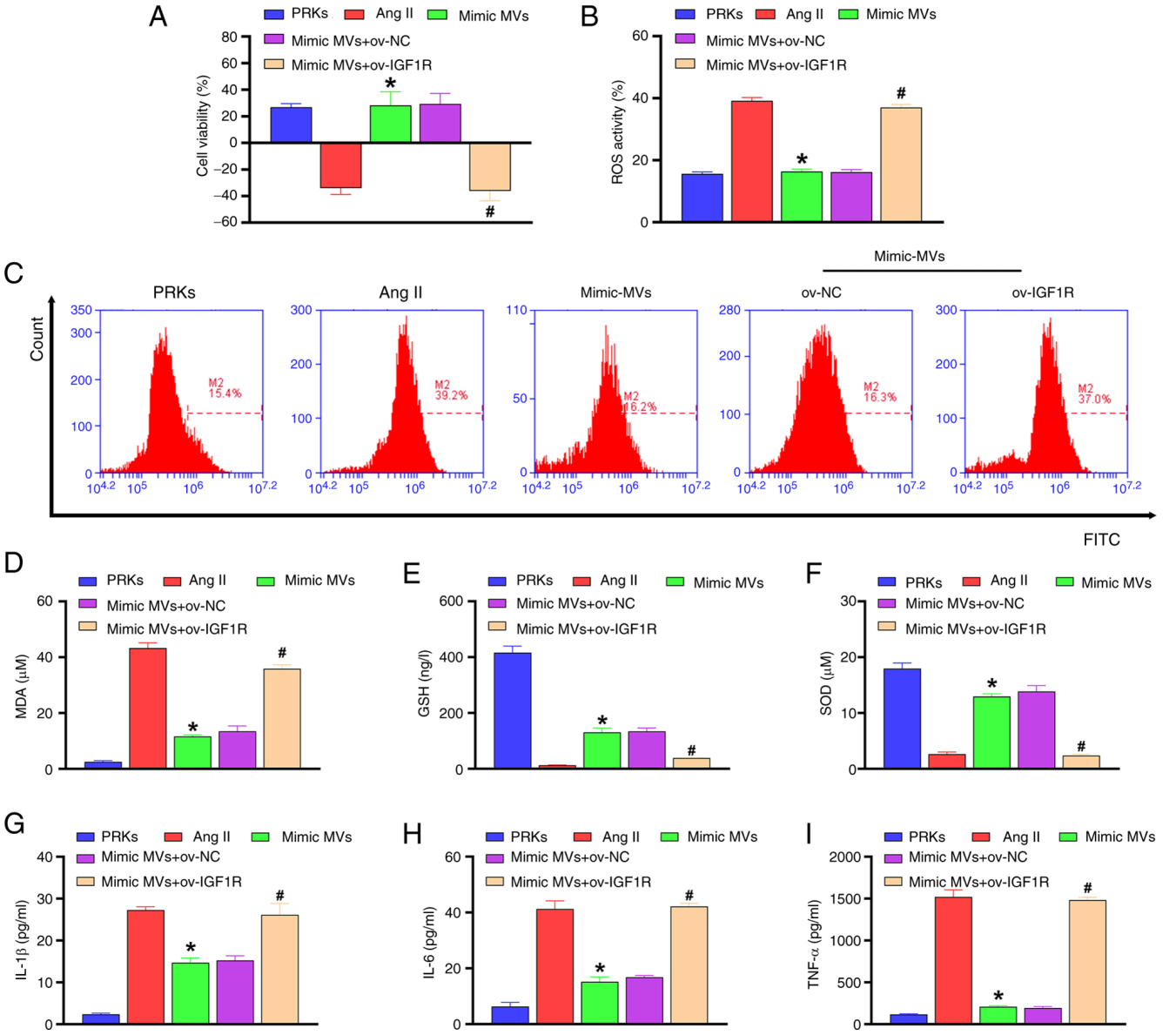

Figure 4. miR-98-5p/IGF1R axis regulates oxidative stress and inflammation in PRKs induced by Ang II. (A) Cell Counting Kit-8 analysis determined the combined effects of miR-98-5p-MVs and IGF1R on the cell viability of PRKs treated with Ang II (n=3). (B and C) Flow cytometry analysis determined the combined effects of miR-98-5p-MVs and IGF1R on Ang II-induced ROS generation in PRKs (n=3). ELISA analysis determined the combined effect of miR-98-5p-MVs on the levels of (D) MDA, (E) GSH and (F) SOD produced by PRKs treated with Ang II (n=3). ELISA analysis determined the combined effects of miR-98-5p-MVs and IGF1R on the levels of (G) IL-1β, (H) IL-6 and (I) TNF-α secreted by PRKs treated with Ang II (n=3). *P<0.05 vs. Ang II; #P<0.05 vs. mimic-MVs + ov-NC. IGF1R, insulin-like growth factor 1 receptor; Ang II, Angiotensin II; ROS, reactive oxygen species; EPCs, endothelial progenitor cells; PRKs, primary renal kidney cells; MVs, microvesicles; MDA, malondialdehyde; GSH, glutathione; SOD, superoxide dismutase; NC, negative control; ov, overexpression; miR, microRNA.

NC. However, when mutant IGF1R was co-transfected with miR-98-5p mimic, the luciferase activity was not significantly different from that of the mimic NC co-transfection group (Fig. 3C). Additionally, the overexpression of IGF1R did not affect the expression of miR-98-5p (Fig. 3D). These results suggested that miR-98-5p directly targets IGF1R. Moreover, the co-culture of PRKs with EPCs or EPC supernatant reduced the expression of IGF1R compared with Ang II group, and under the action of EPC-MVs the expression of IGF1R was reduced compared with Ang II group (Fig. 3E).

miR-98-5p/IGF1R regulates the PI3K/Akt/eNOS signaling pathway. Western blot analysis revealed that compared with the Ang II group, EPC-MVs and miR-98-5p mimic-MVs increased the phosphorylation levels of PI3K/Akt/eNOS and reduced the protein level of IGF1R, while miR-98-5p inhibitor-MVs reduced the phosphorylation levels of PI3K/Akt/eNOS and increased the protein level of IGF1R (Fig. 3F). In order to explore the mechanism of IGF1R in PRKs, a plasmid overexpressing IGF1R was constructed and transfected into PRKs. RT-qPCR results revealed that the expression of IGF1R in the ov-IGF1R group increased compared with the ov-NC group (Fig. 3G), confirming the transfection efficiency of the IGF1R plasmid. Subsequently, western blot analysis showed that miR-98-5p mimic-MVs decreased the level of IGF1R protein and increased the levels

of phosphorylation of PI3K/Akt/eNOS compared with the Ang II group. The effects were reversed by ov-IGF1R (Fig. 3H). Compared with the Ang II group, miR-98-5p mimic-MVs protected PRKs from decreased viability (Fig. 4A), oxidative stress [ROS (Fig. 4B, C) and MDA (Fig. 4D) levels decreased, whereas GSH (Fig. 4E) and SOD (Fig. 4F) levels increased] and inflammatory response [IL-1β (Fig. 4G), IL-6 (Fig. 4H) and TNF-α (Fig. 4I)] induced by Ang II. However, overexpression of IGF1R reversed the protective effect of miR-98-5p mimic-MVs on PRKs.

Discussion

In the present study, it was demonstrated for the first time to the best of our knowledge, that EPC-MVs with high levels of miR-98-5p can protect PRKs from Ang II-induced cell damage.

EPCs can effectively protect from renal function deterioration in CKD (40) and play an important role in maintaining vascular integrity, repairing endothelial injury and improving organ function (41). Recent evidence shows that EPCs may play a protective role by secreting MVs (42). MVs are important mediators of intercellular communication (43) and are detached from the cell surface after activation, stress or apoptosis (44). MVs have anti-inflammatory, anticoagulant and angiogenic effects (45,46), improve endothelial function and alleviate endothelial dysfunction induced by oxidative stress (47). As the damaged kidney can no longer effectively filter out the metabolic waste in the blood, which eventually leads to the occurrence of kidney disease, the GEO analysis in the current study used diabetic rats based on the possibility of diabetic rats suffering from kidney disease (48). One of the main conclusions of the current study is that after the successful establishment of the Ang II-induced PRK injury model, EPC-MVs suppressed the reduction of PRK viability induced by Ang II, as well as the promotion of oxidative stress and inflammation. This result is similar to those in previous studies (49,50).

Dysregulated miR-98-5p expression has been reported to play a key role in the progression of several diseases, such as oral squamous cell carcinoma (51) and bronchial asthma (52). Kokkinopoulou *et al* (53) demonstrated that low levels of miR-98-5p adversely affected the treatment of patients with diabetes, and the results of the GEO data analysis in the present study support this view that the expression of miR-98-5p is downregulated in diabetic rats. In the current study, it was found that miR-98-5p mimic enhanced EPC-MVs-induced viability of PRKs, whereas miR-98-5p inhibitor showed the opposite effect, which was consistent with the research by Kokkinopoulou *et al* (53). In addition, miR-98-5p MVs also reversed the Ang II-induced increase of ROS, MDA, IL-1β, IL-6 and TNF-α levels, as well as the decrease of GSH and SOD levels. Therefore, the potential mechanism of the protective effect of miR-98-5p MVs on PRKs may involve the regulation of oxidative stress and inflammation.

The PI3K/Akt/eNOS signaling pathway is closely related to cell inflammation, viability, endothelial injury and dysfunction (54-56). Our previous study showed that EPC-MVs protect cardiomyocytes from Ang II-induced apoptosis by activating the PI3K/Akt/eNOS signaling pathway (38). In the current study, the mechanism by which miR-98-5p regulates the PI3K/Akt/eNOS signaling pathway was further explored. Through combined analysis of the TargetScan database and KEGG, the IGF1R gene was identified as a potential target gene for miR-98-5p. Subsequent results showed that miR-98-5p directly targets IGF1R and regulates the phosphorylation level of PI3K/Akt/eNOS through IGF1R. Consistently, the overexpression of IGF1R reversed the promotive effect of miR-98-5p mimic-MVs on PRK viability and its inhibitory effect on oxidative stress and inflammation. This result indicates that miR-98-5p regulates the IGF1R/PI3K/Akt/eNOS axis and inhibits the effect induced by Ang II, thereby protecting PRKs.

A limitation of the present study is whether EPC-MVs can protect against kidney injury in animal models of hypertensive nephropathy, and therefore the mechanism of EPC-MVs needs to be further elucidated. Secondly, changes in various signaling pathways, especially inflammation or related pathways, have not been further explored in the current study. Finally, the intracellular distribution of miRNA could be further explored using fluorescence *in situ* hybridization, which was not developed in the present study. These limitations will be the focus of future research.

In summary, miR-98-5p, which is present in high levels in EPC-MVs, protected PRKs from Ang II-induced injury by activating the PI3K/Akt/eNOS signaling pathway and inhibiting oxidative stress and inflammation. Therefore, the current study provides a solid theoretical basis for the potential treatment of hypertensive nephropathy.

Acknowledgements

Not applicable.

Funding

The current study was supported by the Finance Science and Technology Projects of Hainan Province (grant no. ZDYF2019193), the National Natural Science Foundation of China (grant no. 8156020231) and the CAMS Innovation Fund for Medical Sciences (grant no. 2019-I2M-5-023).

Availability of data and materials

The datasets used and/or analyzed during the current study are available from the corresponding author on reasonable request.

Authors' contributions

HM, ZH and SG conceived and designed the study. XZ, YuaZ, JC and MC performed the experiments. YunZ, YS, BW and YL collected and analyzed experimental data. HM and ZH confirm the authenticity of all the raw data. All authors have read and approved the final manuscript.

Ethics approval and consent to participate

Animal experiments were approved by the Animal Care and Use Committee of Hainan Medical University (Haikou, China; approval no. HYLL-2021-053).

Patient consent for publication

Not applicable.

Competing interests

The authors declare that they have no competing interests.

References

1. Hart PD and Bakris GL: Hypertensive nephropathy: Prevention and treatment recommendations. Expert Opin Pharmacother 11: 2675-2686, 2010.
2. Hu H, Jiang C, Li R and Zhao J: Comparison of endothelial cell- and endothelial progenitor cell-derived exosomes in promoting vascular endothelial cell repair. Int J Clin Exp Pathol 12: 2793-2800, 2019.
3. Naito H, Iba T and Takakura N: Mechanisms of new blood-vessel formation and proliferative heterogeneity of endothelial cells. Int Immunol 32: 295-305, 2020.
4. Di Marco GS, Rustemeyer P, Brand M, Koch R, Kentrup D, Grabner A, Greve B, Wittkowski W, Pavenstadt H, Hausberg M, *et al*: Circulating endothelial progenitor cells in kidney transplant patients. PLoS One 6: e24046. 2011.
5. Panagiotou N, Davies RW, Selman C and Shiels PG: Microvesicles as vehicles for tissue regeneration: Changing of the guards. Curr Pathobiol Rep 4: 181-187, 2016.
6. Ranghino A, Cantaluppi V, Grange C, Vitillo L, Fop F, Biancone L, Deregibus MC, Tetta C, Segoloni GP and Camussi G: Endothelial progenitor cell-derived microvesicles improve neovascularization in a murine model of hindlimb ischemia. Int J Immunopathol Pharmacol 25: 75-85, 2012.
7. Zhang M, Malik AB and Rehman J: Endothelial progenitor cells and vascular repair. Curr Opin Hematol 21: 224-228, 2014.
8. El-Shoura EAM, Messiha BAS, Sharkawi SMZ and Hemeida RAM: Perindopril ameliorates lipopolysaccharide-induced brain injury through modulation of angiotensin-II/angiotensin-1-7 and related signaling pathways. Eur J Pharmacol 834: 305-317, 2018.
9. Jia N, Dong P, Ye Y, Qian C and Dai Q: Allopurinol attenuates oxidative stress and cardiac fibrosis in angiotensin II-induced cardiac diastolic dysfunction. Cardiovasc Ther 30: 117-123, 2012.
10. Zhang H, Zhang S, Jia L and Li H: MyD88 overexpression deteriorates Ang-II-induced ED via upregulating MPO and COX2 and downregulating eNOS in the corpus cavernosum of rats. J Cell Biochem 28: 10.1002/jcb.27987, 2018.
11. Zhang L, Du J, Hu Z, Han G, Delafontaine P, Garcia G and Mitch WE: IL-6 and serum amyloid A synergy mediates angiotensin II-induced muscle wasting. J Am Soc Nephrol 20: 604-612, 2009.
12. Zhang LL, Huang S, Ma XX, Zhang WY, Wang D, Jin SY, Zhang YP, Li Y and Li X: Angiotensin(1-7) attenuated angiotensin II-induced hepatocyte EMT by inhibiting NOX-derived H2O2-activated NLRP3 inflammasome/IL-1beta/Smad circuit. Free Radic Biol Med 97: 531-543, 2016.
13. Liu YS, Yang Q, Li S, Luo L, Liu HY, Li XY and Gao ZN: Luteolin attenuates angiotensin IIinduced renal damage in apolipoprotein Edeficient mice. Mol Med Rep 23: 157, 2021.
14. Mohammed-Ali Z, Cruz GL, Lu C, Carlisle RE, Werner KE, Ask K and Dickhout JG: Development of a model of chronic kidney disease in the C57BL/6 mouse with properties of progressive human CKD. Biomed Res Int 2015: 172302. 2015.
15. Souza ACP, Tsuji T, Baranova IN, Bocharov AV, Wilkins KJ, Street JM, Alvarez-Prats A, Hu X, Eggerman T, Yuen PST and Star RA: TLR4 mutant mice are protected from renal fibrosis and chronic kidney disease progression. Physiol Rep 3: 12558, 2015.
16. Correia de Sousa M, Gjorgjieva M, Dolicka D, Sobolewski C and Foti M: Deciphering miRNAs' action through miRNA editing. Int J Mol Sci 20: 6249, 2019.
17. Zhu Y, Xu J, Liang W, Li J, Feng L, Zheng P, Ji T and Bai S: MiR-98-5p alleviated epithelial-to-mesenchymal transition and renal fibrosis via targeting hmga2 in diabetic nephropathy. Int J Endocrinol 2019: 4946181. 2019.
18. Fabian MR, Sonenberg N and Filipowicz W: Regulation of mRNA translation and stability by microRNAs. Annu Rev Biochem 79: 351-379, 2010.
19. Zhang Y, Sun Y, Peng R, Liu H, He W, Zhang L, Peng H and Zhang Z: The long noncoding rna 150Rik promotes mesangial cell proliferation via miR-451/IGF1R/p38 MAPK signaling in diabetic nephropathy. Cell Physiol Biochem 51: 1410-1428, 2018.
20. Lan S and Albinsson S: Regulation of IRS-1, insulin signaling and glucose uptake by miR-143/145 in vascular smooth muscle cells. Biochem Biophys Res Commun 529: 119-125, 2020.
21. Tiwari A, Mukherjee B and Dixit M: MicroRNA key to angiogenesis regulation: MiRNA biology and therapy. Curr Cancer Drug Targets 18: 266-277, 2018.
22. Saliminejad K, Khorshid HR, Fard SS and Ghaffari SH: An overview of microRNAs: Biology, functions, therapeutics, and analysis methods. J Cell Physiol 234: 5451-5465, 2019.
23. Olejniczak M, Kotowska-Zimmer A and Krzyzosiak W: Stress-induced changes in miRNA biogenesis and functioning. Cell Mol Life Sci 75: 177-191, 2018.
24. Kolluru GK, Siamwala JH and Chatterjee S: eNOS phosphorylation in health and disease. Biochimie 92: 1186-1198. 2010.
25. Li CY, Wang LX, Dong SS, Hong Y, Zhou XH, Zheng WW and Zheng C: Phlorizin exerts direct protective effects on palmitic acid (PA)-induced endothelial dysfunction by activating the PI3K/AKT/eNOS signaling pathway and increasing the levels of nitric oxide (NO). Med Sci Monit Basic Res 24: 1-9, 2018.
26. Xing Y, Lai J, Liu X, Zhang N, Ming J, Liu H and Zhang X: Netrin-1 restores cell injury and impaired angiogenesis in vascular endothelial cells upon high glucose by PI3K/AKT-eNOS. J Mol Endocrinol 58: 167-177, 2017.
27. Wang Y, Zhang J, Su Y, Wang C, Zhang G, Liu X, Chen Q, Lv M, Chang Y, Peng J, *et al*: MiRNA-98-5p targeting IGF2BP1 induces mesenchymal stem cell apoptosis by modulating PI3K/Akt and p53 in immune thrombocytopenia. Mol Ther Nucleic Acids 20: 764-776, 2020.
28. Zhang D, Mei L, Long R, Cui C, Sun Y, Wang S and Xia Z: RiPerC attenuates cerebral ischemia injury through regulation of miR-98/PIK3IP1/PI3K/AKT signaling pathway. Oxid Med Cell Longev 2020: 6454281, 2020.
29. Van Dyken P and Lacoste B: Impact of metabolic syndrome on neuroinflammation and the blood-brain barrier. Front Neurosci 12: 930, 2018.
30. Yang P, Liang Y, Luo Y, Li Z, Wen Y, Shen J, Li R, Zheng H, Gu HF and Xia N: Liraglutide ameliorates nonalcoholic fatty liver disease in diabetic mice via the IRS2/PI3K/Akt signaling pathway. Diabetes Metab Syndr Obes 12: 1013-1021, 2019.
31. Wu Q and Hu Y: Systematic evaluation of the mechanisms of mulberry leaf (Morus alba Linne) acting on diabetes based on network pharmacology and molecular docking. Comb Chem High Throughput Screen 24: 668-682, 2021.
32. Kobayashi T, Matsumoto T and Kamata K: Possible involvement of IGF-1 receptor and IGF-binding protein in insulin-induced enhancement of noradrenaline response in diabetic rat aorta. Nihon Yakurigaku Zasshi 122 (Suppl): 40P-42P, 2003.
33. Tan YS and Lei YL: Isolation of tumor-infiltrating lymphocytes by ficoll-paque density gradient centrifugation. Methods Mol Biol 1960: 93-99, 2019.
34. Gyabaah K, Aboushwareb T, Souza NG, Yamaleyeva L, Varner A, Wang HJ, Atala A and Yoo JJ: Controlled regulation of erythropoietin by primary cultured renal cells for renal failure induced anemia. J Urol 188: 2000-2006, 2012.
35. Elliget KA and Trump BF: Primary cultures of normal rat kidney proximal tubule epithelial cells for studies of renal cell injury. In Vitro Cell Dev Biol 27A: 739-748, 1991.
36. Nair AR, Ebenezer PJ, Saini Y and Francis J: Angiotensin II-induced hypertensive renal inflammation is mediated through HMGB1-TLR4 signaling in rat tubulo-epithelial cells. Exp Cell Res 335: 238-247, 2015.
37. Giles EM, Godbout C, Chi W, Glick MA, Lin T, Li R, Schemitsch EH and Nauth A: Subtypes of endothelial progenitor cells affect healing of segmental bone defects differently. Int Orthop 41: 2337-2343, 2017.
38. Gu S, Zhang W, Chen J, Ma R, Xiao X, Ma X, Yao Z and Chen Y: EPC-derived microvesicles protect cardiomyocytes from Ang II-induced hypertrophy and apoptosis. PLoS One 9: e85396, 2014.
39. Livak KJ and Schmittgen TD: Analysis of relative gene expression data using real-time quantitative PCR and the 2(-Delta Delta C(T)) method. Methods 25: 402-408, 2001.
40. Sung PH, Chen KH, Li YC, Chiang JY, Lee MS and Yip HK: Sitagliptin and shock wave-supported peripheral blood derived endothelial progenitor cell therapy effectively preserves residual renal function in chronic kidney disease in rat-role of dipeptidyl peptidase 4 inhibition. Biomed Pharmacother 111: 1088-1102, 2019.

41. Zhou Y, Li P, Goodwin AJ, Cook JA, Halushka PV, Chang E and Fan H: Exosomes from endothelial progenitor cells improve the outcome of a murine model of sepsis. Mol Ther 26: 1375-1384, 2018.
42. Zeng W, Lei Q, Ma J, Gao S and Ju R: Endothelial progenitor cell-derived microvesicles promote angiogenesis in rat brain microvascular endothelial cells in vitro. Front Cell Neurosci 15: 638351. 2021.
43. Soni S, Wilson MR, O'Dea KP, Yoshida M, Katbeh U, Woods SJ and Takata M: Alveolar macrophage-derived microvesicles mediate acute lung injury. Thorax 71: 1020-1029. 2016.
44. Watanabe K: Bacterial membrane vesicles (MVs): Novel tools as nature- and nano-carriers for immunogenic antigen, enzyme support, and drug delivery. Appl Microbiol Biotechnol 100: 9837-9843, 2016.
45. Jaimes Y, Naaldijk Y, Wenk K, Leovsky C and Emmrich F: Mesenchymal stem cell-derived microvesicles modulate lipopolysaccharides-induced inflammatory responses to microglia cells. Stem Cells 35: 812-823, 2017.
46. Zhang Y, Liu D, Chen X, Li J, Li L, Bian Z, Sun F, Lu J, Yin Y, Cai X, *et al*: Secreted monocytic miR-150 enhances targeted endothelial cell migration. Mol Cell 39: 133-144, 2010.
47. Zeng W, Lei Q, Ma J and Ju R: Effects of hypoxic-ischemic pre-treatment on microvesicles derived from endothelial progenitor cells. Exp Ther Med 19: 2171-2178, 2020.
48. Tonneijck L, Muskiet MH, Smits MM, van Bommel EJ, Heerspink HJ, van Raalte DH and Joles JA: Glomerular hyperfiltration in diabetes: Mechanisms, clinical significance, and treatment. J Am Soc Nephrol 28: 1023-1039. 2017.
49. Du Y, Han J, Zhang H, Xu J, Jiang L and Ge W: Kaempferol prevents against ang II-induced cardiac remodeling through attenuating ang II-induced inflammation and oxidative stress. J Cardiovasc Pharmacol 74: 326-335, 2019.
50. Singh MV, Cicha MZ, Meyerholz DK, Chapleau MW and Abboud FM: Dual activation of TRIF and MyD88 adaptor proteins by angiotensin II evokes opposing effects on pressure, cardiac hypertrophy, and inflammatory gene expression. Hypertension 66: 647-656, 2015.
51. Niu X, Yang B, Liu F and Fang Q: LncRNA HOXA11-AS promotes OSCC progression by sponging miR-98-5p to upregulate YBX2 expression. Biomed Pharmacother 121: 109623, 2020.
52. Du J, Wu H and Wu Y: MiR-98-5p may be a biomarker for screening bronchial asthma in children by targeting IL-13. Clin Lab 65: 10.7754, 2019.
53. Kokkinopoulou I, Maratou E, Mitrou P, Boutati E, Sideris DC, Fragoulis EG and Christodoulou MI: Decreased expression of microRNAs targeting type-2 diabetes susceptibility genes in peripheral blood of patients and predisposed individuals. Endocrine 66: 226-239, 2019.
54. Duan MX, Zhou H, Wu QQ, Liu C, Xiao Y, Deng W and Tang QZ: Andrographolide protects against HG-induced inflammation, apoptosis, migration, and impairment of angiogenesis via PI3K/AKT-eNOS signalling in HUVECs. Mediators Inflamm 2019: 6168340, 2019.
55. Li JB, Wang HY, Yao Y, Sun QF, Liu ZH, Liu SQ, Zhuang JL, Wang YP and Liu HY: Overexpression of microRNA-138 alleviates human coronary artery endothelial cell injury and inflammatory response by inhibiting the PI3K/Akt/eNOS pathway. J Cell Mol Med 21: 1482-1491, 2017.
56. Zhang Z and Zhang D: (-)-Epigallocatechin-3-gallate inhibits eNOS uncoupling and alleviates high glucose-induced dysfunction and apoptosis of human umbilical vein endothelial cells by PI3K/AKT/eNOS pathway. Diabetes Metab Syndr Obes 13: 2495-2504, 2020.

This work is licensed under a Creative Commons Attribution-NonCommercial-NoDerivatives 4.0 International (CC BY-NC-ND 4.0) License.